THE ROLE OF KELVIN WAVE ACTIVITY ON CONVECTION AND RAINFALL
OVER TROPICAL AFRICA

Ademe Mekonnen[*]
State University of New York at Albany, Albany, NY

1. INTRODUCTION

Tropical Africa is known to be dominated by westward moving African easterly waves (e.g., Carlson 1969, Reed et al 1977). Observational studies based on time filtering analysis have also indicated the presence of eastward moving convective systems (e.g., Mekonnen et al 2006; hereafter MTA06), from west and central Africa towards eastern Africa during the boreal summer season. MTA06 speculated that these convective systems may be associated with Kelvin wave activity. However, this has not yet been addressed in detail. It is the aim of this study to shed some light on this issue.

In the literature, considerable effort has been made to study the role of Kelvin wave activity on convection over the Pacific. Using satellite observed cloud data and Kinematic and thermodynamic fields, Takayabu and Murakami (1991) and Takayabu (1994) demonstrated that eastward movement of cloud clusters over the western Pacific are associated with the Kelvin wave activity. More recently, in a case study that utilizes observational and reanalysis data sets, Straub and Kiladis (2002; hereafter SK02) showed that the Kelvin wave disturbance strongly controls the local convective activity over the equatorial Pacific near the date line. They demonstrated that convective activity enhances as the Kelvin wave approaches the region, while convection weakens and stratiform clouds dominate when the wave envelope passed the region. Also, using an observational data set from TRMM KWAJEX experiment (for the period 23 July-15 September 1999) for western and central North Pacific, Sobel et al (2004) reported that rainfall events during the early days of the experiment period were associated with the passage of a Kelvin wave. However, they also noted that rainfall during some of the days were associated with either mixed-Rossby gravity waves or tropical disturbance (TD)-type waves.

We know little about the synoptic scale Kelvin wave activity and its potential modulation of rainfall and convection over tropical Africa. On an intraseasonal time scale, Mathews (2004) studied the impact of Kelvin wave activity triggered as a response to intraseasonal oscillation of a suppressed convection over the western Pacific region and that reached West Africa 20 days after its initiation. He concluded that the impact of the approaching Kelvin wave towards West Africa is to increase the boundary layer monsoon flow and moisture from the southern Atlantic Guinea coast, which contributed to enhanced convection.

This study will use satellite observed brightness temperature data and examines, in more detail, the impact of synoptic scale Kelvin wave activity on convection. A case study will also be presented to illustrate the results found based on composite analysis.

This paper is organized as follows. Section 2 provides a brief description of the data used and methodologies that will be employed. Section 3 discusses results found in a climatological context. A case study that illustrates the association between Kelvin wave activity and convection and rainfall will be provided in section 4. Section 5 offers a brief summary of the results.

2. DATA AND METHODOLOGY

To achieve our objective we will use brightness temperature (T_B) from Cloud Archive User Service (CLAUS) of the European Union to investigate the characteristics of convection, and the European center for Medium Weather Forecast (ECMWF) 40-year reanalysis (ERA40) data to study the dynamical measures. The period of study is 1984-2000 and the results are mainly for the July-September (JAS) period.

CLAUS T_B is a high resolution, global 0.5° grid and 3-hourly, data and compiled from multiple satellite observations (both geostationary and polar orbiting) in the infra-red window of 11-12μm. The CLAUS data has been described in detail by Hodges et al (2000) and it was successfully applied by Yang and Slingo (2001) and MTA06.

The ERA40 is a global 2.5° horizontal grid and 6-hourly data set and has multiple vertical levels (we use 00 and 12UTC). Admittedly, observational data is sparse over Africa. However, we are confident that this data is adequate for the scale of analysis we are interested in this work (see Reed et al 1998 and

[*] Corresponding author's address: Ademe Mekonnen, SUNY at Albany, Dep't of Atmospheric Science, 1400 Washington Ave., Albany, NY 12222. E-mail: ademe@atmos.albany.edu

Tompkins et al 2005 for details).

The eastward propagating wave signature of the T_B field is isolated using space-time filtering in the Kelvin wave range following Wheeler and Kiladis (1999; hereafter WK99). Details of the space-time filtering technique is described in detail in WK99 and Wheeler et al (2000; hereafter WKW00). The filtering window for the Kelvin wave range is the period 2.5-17 days, and wave number 1-14, similar to that of SK02 and Roundy and Frank (2004). WK99 and WKW00 have performed the filtering for the symmetric component of the outgoing longwave radiation (OLR) field. However, here the filtering is carried out on the total T_B field, without separating the field into symmetric and antisymmetric components, as in SK02. The basis for this is that the convective peaks over tropical Africa and other tropical regions during the boreal summer are located well to the north of the equator, along the Inter-Tropical Convergence Zone (ITCZ). We expect that the eastward moving convective variances to be nearly symmetric with the mean location of the ITCZ rather than with equator. The filtered T_B field in the above range represents the convectively coupled Kelvin wave (see WK99, WKW00 and SK02 for detailed discussion on this).

In addition, a linear regression technique has been applied to form composite structures of dynamical and convective fields in order to closely investigate the interaction between Kelvin wave and convection, following WKW00. As a first step, we objectively choose $10^oN, 20^oE$ as a base point (reference point), a location where Kelvin filtered T_B variance is a maximum. The time series (or reference time series) at this point is derived from the Kelvin filtered data. Then, the reference timeseries will be used for regression, at various time lags, onto a total data field. Our approach is slightly different from that of WKW00. While we use the twice daily JAS time series for the regression analysis, WKW00 based their analysis on daily averages of the January-December time series. They chose their base point reference OLR daily time series in such a way that the daily variance exceeds the averaged variance of all months. WKW00 indicated that this maximizes the signal-to-noise ratio. Regression results are tested for significance. To compute the significance levels, we first find the decorrelation time scale. The decorrelation time scale is calculated using Eq. 1 of Livezey and Chen (1983) and the number of degrees of freedom is computed using Eq. 2 of Livezey and Chen (1983). Then, assuming deviations from the regression for the dependent variable are "normally" distributed, the significance level of a given correlation coefficient is determined based on the two-tailed T-test (see also WKW00).

3. RESULTS AND DISCUSSION

Figure 1 shows the Kelvin wave filtered T_B for the global tropics. Peak activities are located over tropical Africa centered at $10^oN, 20^oE$, equatorial Indian ocean centered at 90^oE, tropical Pacific between 5^oN to 12^oN and stretching towards tropical Atlantic near 10^oN. The maximum activities are located north of the equator in the vicinity of the summer time ITCZ, except over the Indian ocean.

We now consider regression techniques, following WKW00, to illustrate the interaction between Kelvin wave activity (represented by base point Kelvin filtered T_B; K-T_B for short) and various convective and dynamical fields. Our focus will be mainly over tropical Africa and the Atlantic.

Figure 2 shows the Hovmoller diagram of the composite of K-T_B at the base point regressed onto T_B (shaded in color), and onto 925 hPa geopotential height (in units of m^2s^{-2}, contours) and 925 hPa zonal winds (red contours). The latitudinal average is 7°-12^oN, a region of peak variance activity (see fig. 1). An enhanced convective packet propagates eastward from the central Atlantic towards 40^oE (eastern Ethiopian highlands) at a phase speed of about $15.4ms^{-1}$. This is remarkably similar to the results of WKW00, who showed a propagating envelope of convectively coupled Kelvin wave OLR between equatorial Africa and the date line with a similar speed. However, we note that their results are an average of all months while our study is based on JAS. The eastward moving convective anomaly decays east of 40^oE, but seems to appear over the northern tropical Indian ocean.

Westerly winds are collocated with enhanced convective anomaly, especially between coastal West Africa and eastern Africa, while easterlies are dominant over suppressed convective areas. The zonal wind anomalies are also roughly in phase with the geopotential height anomalies, consistent with theory (Matsuno 1966) and in agreement with WKW00. The meridional winds are much weaker than the zonal winds (not shown), as expected for the Kelvin wave. The zonal winds propagate with the same speed as convective anomaly over tropical Africa. Similarly, the geopotential height anomalies propagate eastwards with approximately the same speed as the convective anomalies. Enhanced convective developments are preceded by negative geopotential anomalies, while the positive height anomaly centers are located to the west of the peak convection, consistent with WKW00. Peak convective activities are located under tighter geopotential height gradients, where low- level

westerlies are stronger. These stronger westerly anomalies are moist (oceanic origin; coincide with positive specific humidity) and they help fuel the convection.

The geopotential height and wind anomalies propagate slightly faster over central and eastern Atlantic (~18ms^{-1}). Such a faster eastward propagation of heights and winds farther away from positive convective (negative T_B anomalies) regions is consistent with studies of WKW00 and WK99, who demonstrated that uncoupled Kelvin waves move faster than those coupled waves. Both geopotential height and wind anomalies seem to be weakened between 40°E and 60°E.

Examination of the Hovmoller diagram also reveals that the Kelvin wave has a periodicity of 4-days, consistent with a measure of synoptic scale wave. Along 20°E, for example, a weak convective anomaly is replaced by a strong convective anomaly in about 2 days, and about 2 days later, another weak convective anomaly moves into this location.

In order to get more insight into the nature and structure of the composite anomaly fields, synoptic maps at the upper tropospheric level are considered below.

Figure 3 illustrates the evolution of K-T_B at the base point (10°N,20°E) regressed onto 200-hPa geopotential height and winds, and superimposed with the K-T_B regressed convection, from 4 days before (day - 4) to 2 days after the peak convection at the base point (day 0) for the tropical region between 80°W and 80°E. At day - 4, strong convective anomaly is observed over the eastern Atlantic, near 40°W, within the climatological ITCZ, whereas suppressed convection is located mainly over land between 0° and 10°E. Stronger convection is associated with upper level wind divergence, and suppressed convection is associated with upper level convergence. Positive geopotential height anomalies are located east of the peak convection, somewhat centered near the equator, consistent with WKW00.

At day -2, positive geopotential height anomaly is centered ahead of peak convection, around 15°N and equatorial latitudes. The stronger convective signal has reached West Africa and the peak is centered along the Greenwich meridian and between 10°-15°N. It seems that the convective center moves faster between day -4 and day -2 (~20 ms^{-1}). The geopotential height anomaly has also moved, but slower than the convective and wind fields. At day -1, the peak convection moved farther east and shows two centers: one around 10°N, 12°E and the second near equator and 20°E, with northwest-southeast orientation. Two suppressed convective activities, one to the west of the peak convection over West African coast and eastern Atlantic, and the other to the east over eastern Africa near 10°N, 30°E are seen. The latter is very weak. The geopotential height anomaly center seems to move northeastwards, while the wind pattern appears to show near symmetry about the equator. Between day -2 and day -1, convective propagation and the associated winds have moved slowly (~12 ms^{-1}), as expected for convectively coupled Kelvin wave (WK99, WKW00). Also, geopotential height anomalies propagate at about the same speed (see also fig. 2).

At day 0, the peak convection is located at the base point, as expected, coincident with strong upper level wind divergence (outflow), while positive height anomaly is located 15° to the east of the maximum convection center. The wind pattern shows near symmetry with respect to the equator (c.f. WKW00 and SK02). It should be noted that the positive geopotential height moved northeastwards between day -2 and day 0. At day 1, maximum convection and associated wind divergence are located along 30°E, but the positive height anomaly is situated near the equator. At day 2, convection continues to move eastward, while weakening, and is now located around 10°N, 40°E, over the eastern Ethiopian highlands. Consistent with WKW00 and WK99, convection is essentially asymmetric, while dynamical measures show near symmetry about the equator.

The discussion thus far highlights the composite picture of the nature of convectively coupled Kelvin wave structures over the Atlantic and tropical Africa. The section below expands the discussion based on a case study: a stronger Kelvin wave event that started over eastern tropical Pacific and propagated eastwards across the Atlantic, tropical Africa and Indian ocean and decayed over western Pacific during JAS 1987.

4. CASE STUDY
(a) JAS 1987

Figure 4 shows a Hovmoller diagram of convection (unfiltered T_B) and Kelvin wave filtered T_B (K-T_B) for JAS 1987 and for the region between the date line and 120°E (averaged between 7°-12°N, the latitude of the peak climatological Kelvin wave activity over Africa; see fig. 1). Stronger convective events are shaded ($T_B < 260$K) and the negative K-T_B (stronger wave events) are contoured (positive K-T_B not shown for clarity). Convective activity occupies a much larger area over the eastern and western Pacific basin, while it occupies relatively less area over the Atlantic and tropical Africa. It is seen that the large scale convective envelope is composed of several mesoscale convective systems (MCSs).

While the large scale envelope shows eastward propagation, which may be associated with Kelvin wave activity (e.g., Takayabu and Murakami 1991), the smaller scale MCSs in the convective packet shows a clear westward propagation. Figure 4 also shows a number of coherent Kelvin wave events that start from the eastern Pacific and propagate across the tropical Atlantic and Africa and reaching southeast Asia-western Pacific sector, except the second half of August where wave activity is lacking over tropical Africa. The fact that most of these events can be tracked from central and eastern Pacific suggests that the Kelvin waves that reach Africa are initiated by a large convective activity over the eastern Pacific. This study will focus on the basic issue of how an approaching Kelvin wave activity impacts convective development and rainfall production over tropical Africa, with special emphasis on the eastern part. Mechanisms and basic state conditions associated with Kelvin wave initiation are left for future study.

Here, of particular interest is the stronger Kelvin wave event that started over eastern Pacific around 29 July and that decayed over south east Asia-western Pacific region, near 120^oE, around 18 August 1987 (the event is identified by arrows in fig. 4). This wave travelled about 24000 Km with an average phase speed of about 13 ms^{-1}, and actually peaks over east Africa. Detailed discussion of this event is provided below.

(b) A case of Kelvin wave event and associated convection and rainfall

Figure 5 presents synoptic maps of the evolution of the convectively coupled Kelvin wave phases, unfiltered wind anomaly and unfiltered convection between the eastern Pacific and the eastern India. Shown are deeper convective events (T_B < 260K, shaded), Kelvin wave filtered T_B (contoured; only the enhanced phase is shown for clarity) and 925hPa wind anomaly (vectors; anomalies less than 15% of the maximum wind are masked for clarity). Unfiltered wind anomalies for each time of the day are calculated by subtracting 15 days average wind centered at the same time of the day.

On the 29th of July, a large area of convective activity, oriented southwest-northeast, is seen around 0°- 20^oN, 90°-110^oW, over eastern Pacific, collocated with anomalously strong southwesterly low-level wind. Another convective maximum is also located over and parallel to the central America, oriented southeast-northwest, coincident with southerly-southeasterly winds. Weak convectively coupled Kelvin structure is seen around 5^oN, and slightly to the south of the main convective center. Two days

later (on the 31st), the main convective peak moved slightly north-northeastward towards western Mexico and adjoining eastern tropical North Pacific. The other peak convection moved eastward and northward and now located over eastern extreme parts of the Pacific and western Atlantic, over and around central America. Coincident with the latter peak convection is southeast-northwest extended wind convergence line. An enhanced Kelvin filtered T_B anomaly is seen occupying large area around Panama and northwest Columbia. This indicates that such an eastward propagating Kelvin wave activity may have been triggered by the convection over the eastern Pacific region. Between 8/02 and 8/04 (not shown) Kelvin wave continued to move eastswards into into central Atlantic and convective development was observed to the east of the wave.

By 8/05, the Kelvin wave reaches the eastern Atlantic and organized convective activity is seen over Guinea highlands and at the coast. This is consistent with the case study of SK02 who showed the strengthening of convective activity and organization of convective clouds with the approach of Kelvin wave over central and eastern Pacific. This convective activity over land is enhanced with northerly anomalies. By 8/07, the Kelvin wave reaches around Guinea. The southerly and south-westerly anomalies are to the west of the wave and southerly/southeasterly anomalies seem to dominate on its leading edge. Deep convection is formed between 5°- 15^oN and along 5^oE. The approaching Kelvin wave may have helped convective activity to develop even further. This is consistent with Mathews (2004) who attributed an increasing convective activity over West Africa to a Kelvin wave event.

By 08/09, the Kelvin wave moved farther east, while strengthening, and is now located over the region 5°- 10^oN, 10°-20^oE. By 8/10, the Kelvin wave approaches central Darfur and is collocated with deep convective activity, with low tropospheric southerly anomalies to the south of the system. Another convective development is observed over central Ethiopian highlands. On the 11th, the Kelvin wave moved over the region between south Sudan and Ethiopian highlands. Large convective activity is seen over a wider area coincident with the wave and over the Ethiopian highlands. On this day, rainfall abruptly increased over southern and central Ethiopian highlands (see below), which is the result of intense convection associated with the approach of the Kelvin wave. On the 12th (not shown), the Kelvin wave was located between eastern half of Ethiopia and Somalia while convection is seen over eastern Ethiopian lowlands. In order to better understand the

effect of approaching Kelvin wave on cloudiness and rainfall, an average of 8-rainfall stations located in the region 7°-9^oN, 35°-40^oE over Ethiopian highlands are presented below.

Figure 6 shows the average daily rainfall (bar graph; shaded) and Kelvin wave index (solid line) for August 1987 (correlation = -0.28). The Kelvin wave timeseries is extracted from the same region where the stations are located (spacially averaged). As shown in fig. 5, maximum convective activity in the vicinity Ethiopian highlands was observed on 8/10 and 8/11. This corresponds well with the sudden increase in rainfall. The Kelvin wave index also shows strongly negative values (positive phase) on these days. By 8/12, the wave signal was east of the highlands and convective activity was weaker. The rainfall was also at its minimum.

The conclusion here is that an approaching Kelvin wave helps enhance convective activity and associated rainfall over tropical Africa, particularly over the east. The evidence found in this study strengthens and provides additional support for the earlier findings of SK02, Sobel et al (2004) and Takayabu and Murakami (1991), whose studies were mainly focussed on the Pacific basin. It is also consistent with Mathews (2004), who studied the interaction between Kelvin wave and convection over West Africa on an intraseasonal timescale. Also, the case study presented, for the first time, has important implication for daily to medium range rainfall forecast for Ethiopia and its vicinity, in particular, and to the Horn of Africa in general.

5. SUMMARY

Using a 17-year T_B and ERA40 data sets, the role of Kelvin waves on convective activity and rainfall over tropical Africa has been examined. Based on regression analysis, we have shown an eastward moving convective envelope between central tropical Atlantic ocean and eastern Ethiopia. This envelope propagated with an average speed of about 15ms^{-1}, typical of Kelvin wave phase speed. Enhanced convection is coincident with low-level westerlies, while easterlies precede stronger convection by about 2-days, consistent with WKW00. Positive geopotential height anomalies were mainly to the west of the peak convection (fig. 2). In the vicinity of stronger convection, winds and height anomalies propagate with about the same speed as the convection, indicating stronger convective coupling. Dynamical measures and height anomalies seem to propagate slightly faster in the areas where convection is suppressed or very weak (central and eastern Atlantic), an indication of poor coupling between convection and the dynamics

(WK99, WKW00, SK02). Also, as revealed in this work, convective anomaly over a given region is periodic with 4-days, consistent with a measure of synoptic scale Kelvin wave.

The horizontal structure of the dynamical fields show near symmetric with respect to the equator, while convective measure is essentially asymmetric, consistent with findings of WK99 and WKW00. Stronger convective anomalies have been observed to be collocated with upper level divergence, while positive geopotential height anomalies were located to the east of the peak convection, as expected from linear theory.

A case study approach has been employed to better understand the role of Kelvin waves on convection. The case selected was a strong Kelvin wave event that started near eastern Pacific ocean and culminated over southeast Asia-western Pacific sector. In general, over tropical Africa, convective activity seems to deepen with an approaching Kelvin wave. In particular, an abrupt increase in daily rainfall associated with the positive phase of the Kelvin wave event has been observed over central and southern Ethiopia. Note that this has an important predictive value in short and medium weather forecasting. Also, of particular relevance is to the West African Monsoon Experiment planned to take place in the summer of 2006.

REFERENCES

Carlson, T. N., 1969: Synoptic histories of three African disturbances that developed into Atlantic hurricanes. *Mon. Wea. Rev.*, 97, 256-275.

Hodges, K. I., D. W. Chappell, G. J. Robinson, and G. Yang, 2000: An improved algorithm for generating global window brightness temperatures from multiple satellite infrared imagery. *J. Atmos. Oceanic Technol.*, 17,1296-1312.

Livezey, R. E, and W.Y. Chen, 1983: Statistical field significance and its determination by Monte Carlo technique. *Mon. Wea. Rev.*, 111, 46-59.

Mekonnen, A., C. D. Thorncroft, A. R. Aiyyer, 2006:

Analysis of convection and its association with African easterly waves. *J. Climate* (in press).

Reed, R. J., D. C. Norquist and E. E. Recker, 1977: The structure and properties of African wave disturbances as observed during Phase III of GATE. *Mon. Wea. Rev.*, 105, 317-333

Reed, R. J., E. Klinker, and A. Hollingsworth, 1988: The structure and characteristics of African easterly wave disturbances determined from ECMWF operational analysis/ forecast system. Meteorol. Atmos. Phys., 38, 22-33.

Roundy, P. E., and W. M. Frank, 2004: A climatology of waves in the equatorial region. *J. Atmos. Sci.*, 61, 2105-2132.

Sobel, A. H., S. E. Yuter, C. S. Bretherton, and G.N. Kiladis, 2004: Large-scale Meteorology and deep convection during TRMM KWAJEX. *Mon. Wea. Rev.*, 132, 422-444.

Straub, K. H., and G. N. Kiladis, 2002: Observations of a convectively coupled Kelvin wave in the eastern Pacific ITCZ. *J. Atmos. Sci.*, 59, 30-53.

Takayabu, Y. N. and M. Murakami, 1991: The structure of super cloud clusters observed in 1-20 June 1986 and their relationship to easterly waves. *J. Meteor. Soc. Japan*, 69, 105-125.

Takayabu, Y. N., 1994: Large-scale disturbances associated with equatorial waves. Part I: Spectral features of the cloud disturbances. *J. Meteor. Soc. Japan*, 72, 433-448.

Tompkins, A.M., A. Diongue, D. J. Parker, C. D. Thorncroft 2005, The African easterly jet in the ECMWF Integrated forecast system: 4DVar analysis, Q. J. R. Meteorol. Soc., 131, (in press).

Wheeler, M., and G. N. Kiladis, 1999: Convectively coupled equatorial waves: Analysis of clouds and temperature in the wave-number-frequency domain. *J. Atmos. Sci.*, 56,374-399.

Wheeler, M., G. N. Kiladis, and P. J. Webster, 2000: Large-scale dynamical fields associated with convectively coupled equatorial wave. *J. Atmos. Sci.*, 57,613-635.

Yang, G., and J. Slingo, 2001: The diurnal cycle in the tropics. *Mon. Wea. Rev.*, 129, 784-801.
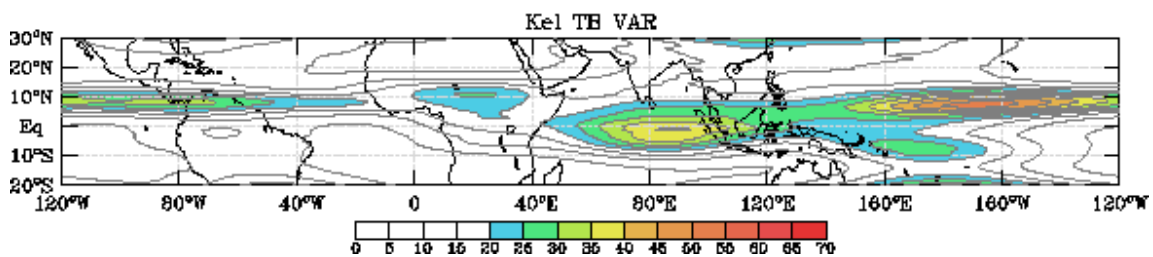
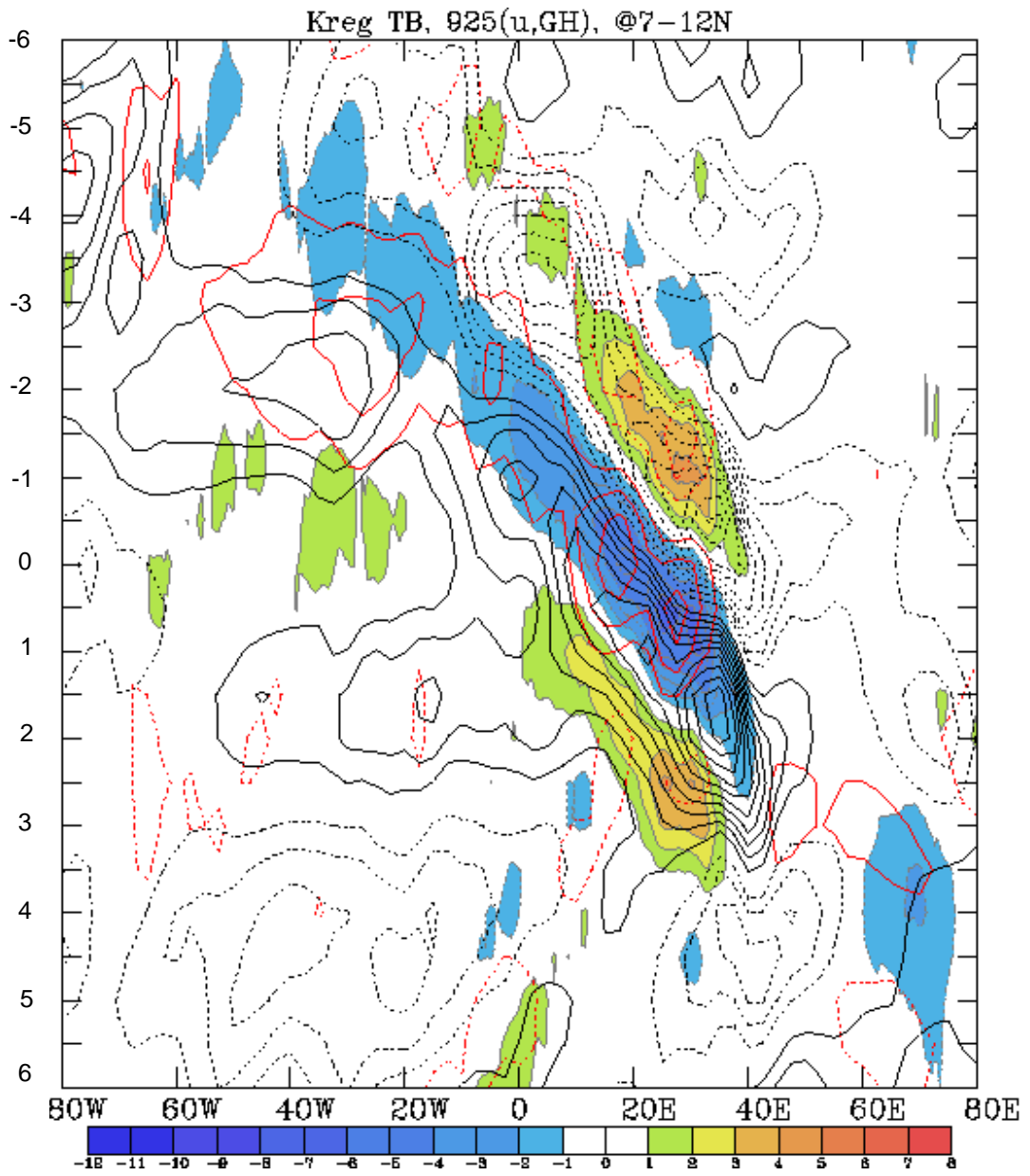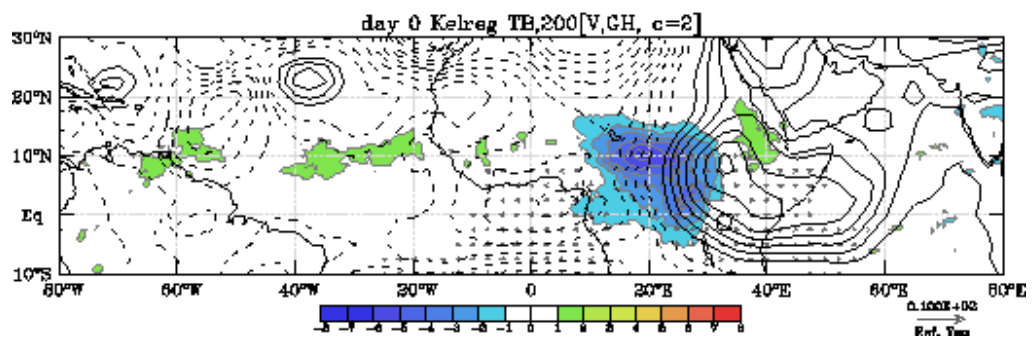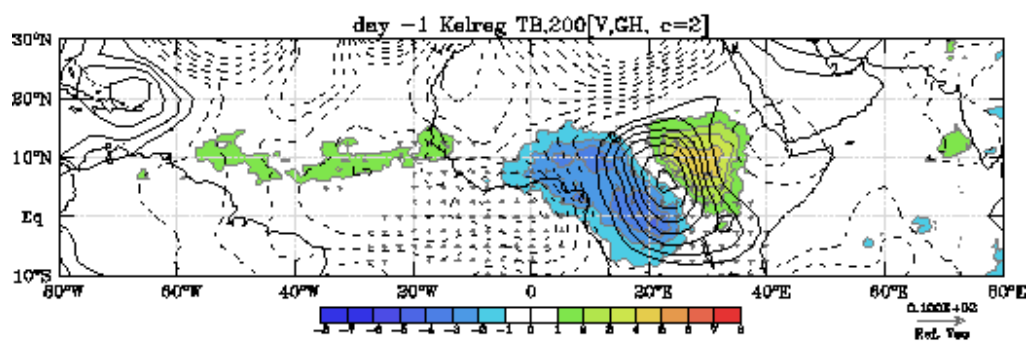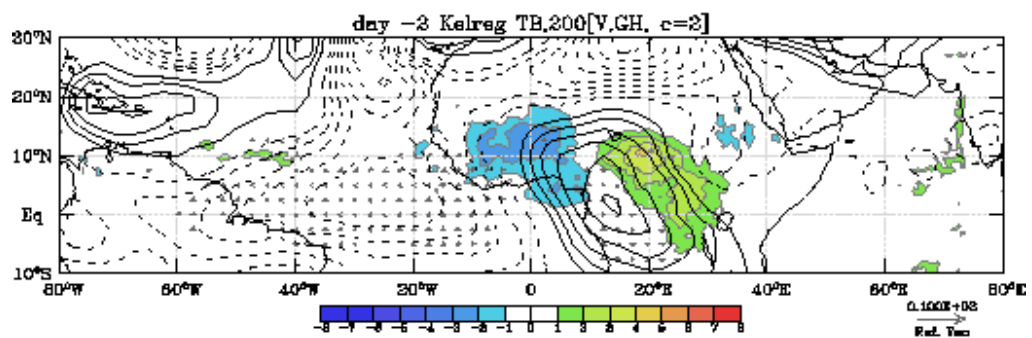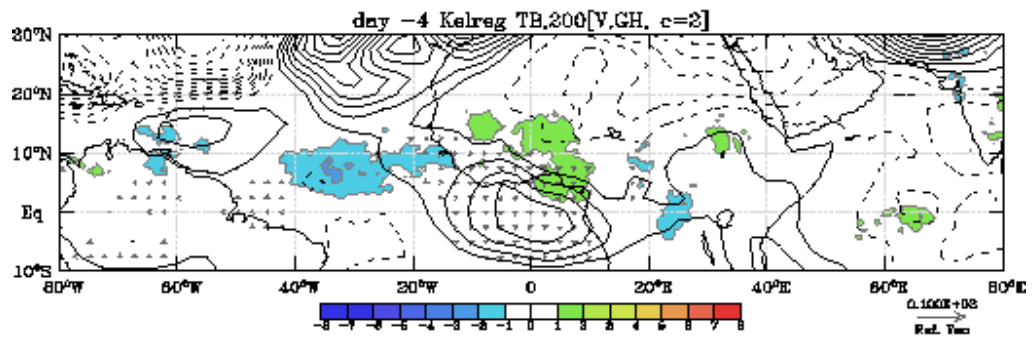Figure 1 : Geographical distribution of Kelvin wave filtered T_B variance (K^2).

Figure 2 : Kelvin filtered T_B regressed onto/ unfiltered T_B (shaded); 925 hPa geopotential height (contoured in black; positives solid, negatives dashed), and 925 hPa zonal wind (contoured in red colour; positives solid and negatives dashed).
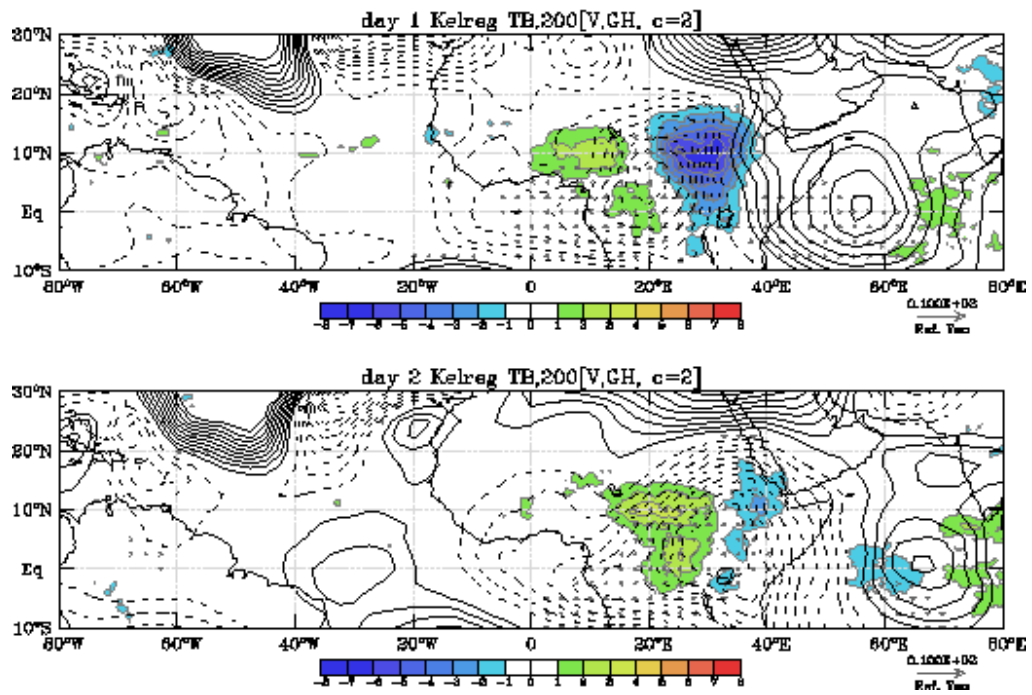
day −4 Kelreg TB,200[V,GH, c=2]

day −3 Kelreg TB,200[V,GH, c=2]

day −1 Kelreg TB,200[V,GH, c=2]

day 0 Kelreg TB,200[V,GH, c=2]

Figure 3 : Synoptic maps from day –4 to day 2 of Kelvin T_B regressed onto unfilterd 200 hPa geopotential height (contours every $2m^2/s^2$), and onto winds (vectorsd). Signficant winds greater than 90% are shown.
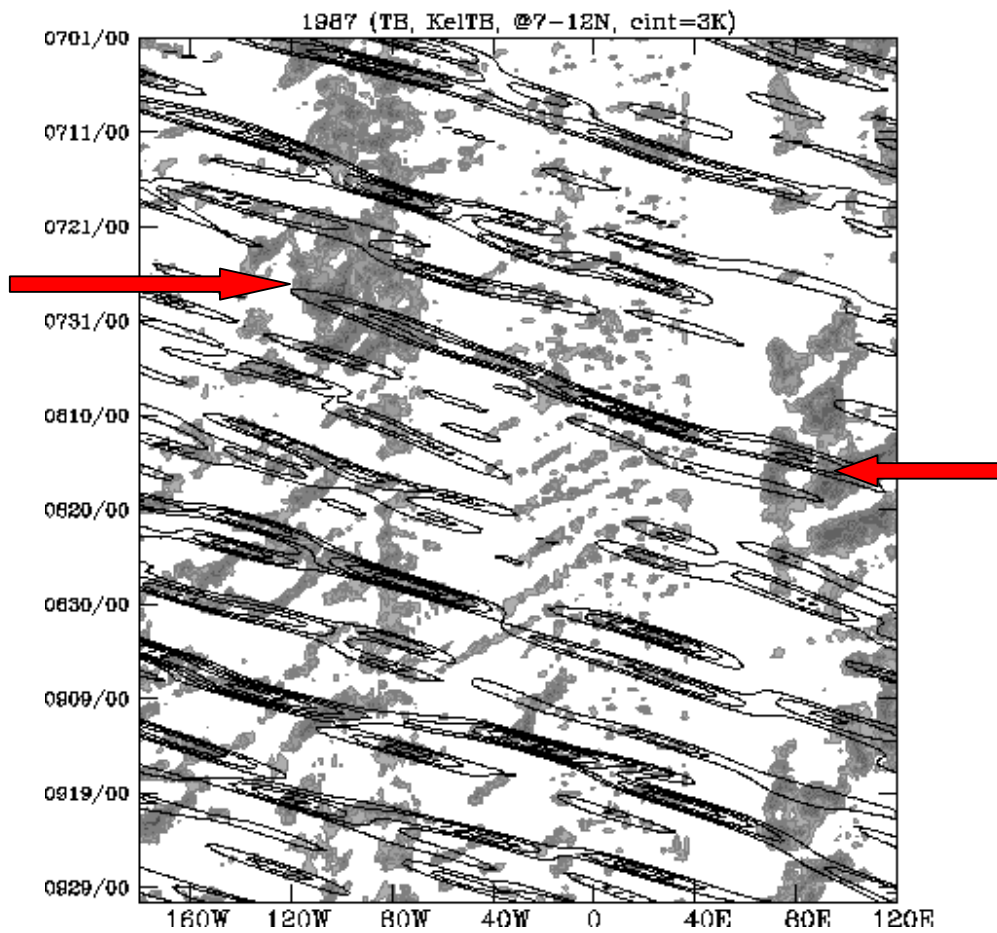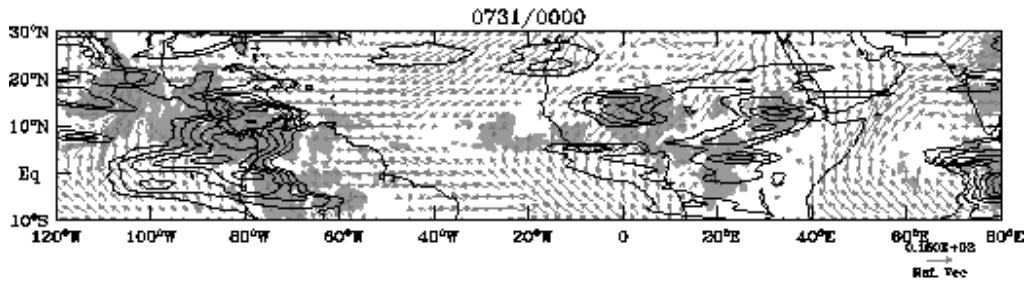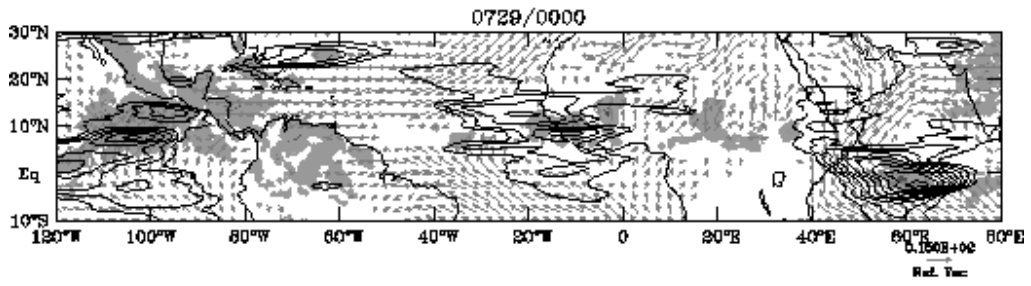
Figure 4 : Hovmoller diagram showing unfiltered T_B (<260K; shaded), and Kelvin filtered T_B (only positive phase is shown. Negative phases are masked for clarity). Arrows show the event selected for the case study (see text)
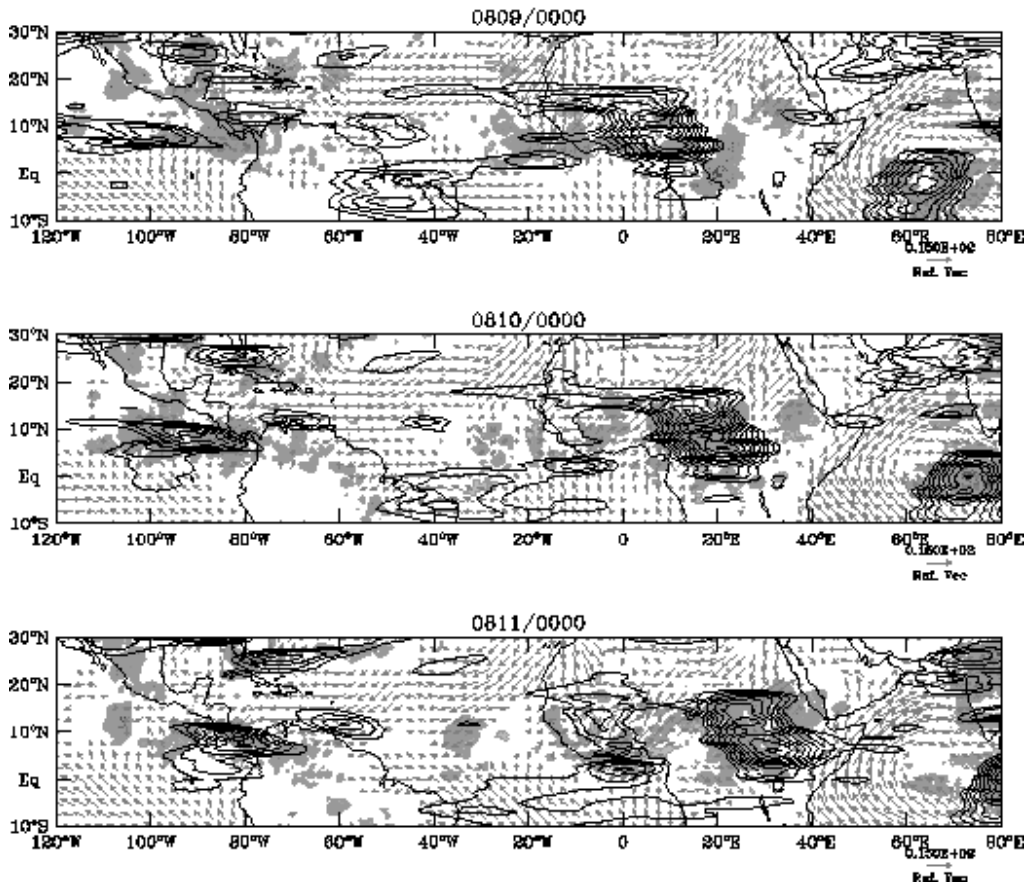
0729/0000

0731/0000

0805/0000

0807/0000
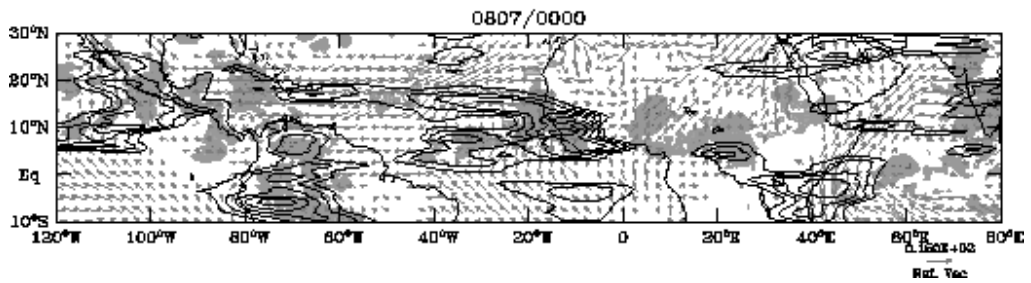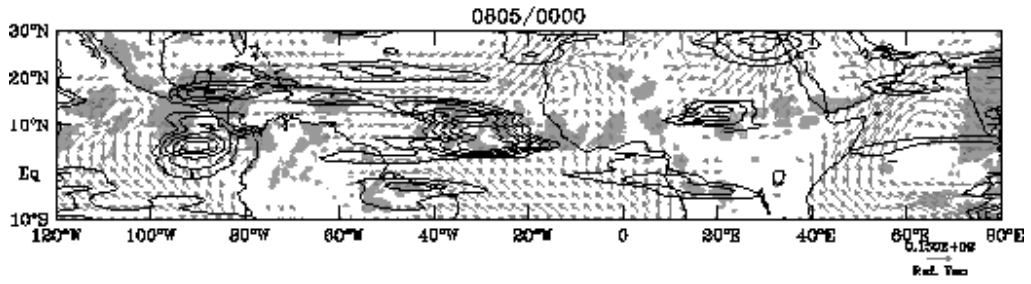
Figure 5 : Synoptic maps of the evolution of Kelvin wave (contoured every 2K, negative phases not shown), unfiltered T_B (shaded, T_B< 260K), 925 hPa unfiltered wind anomaly (winds less than 15% of the maximum wind are masked for clarity).
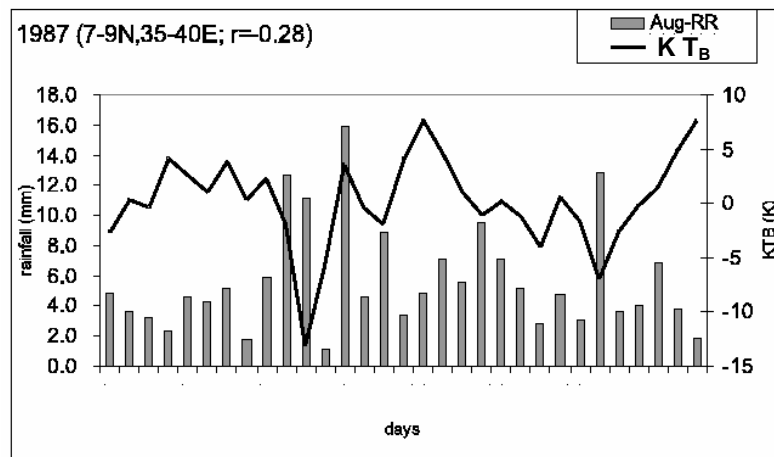

Figure 6 : Average rainfall from 8 stations over central and southern Ethiopia and area averaged Kelvin filtered TB time series for August 1987 (box averaged in 7-9N, 35-40E).